CrossMark

ORIGINAL RESEARCH PAPER

# Influence of soil–structure interaction (structure-to-soil relative stiffness and mass ratio) on the fundamental period of buildings: experimental observation and analytical verification

Wei Xiong[1] · Li-Zhong Jiang[1,2] · Yao-Zhuang Li[1,2]

**Abstract**   In order to investigate the influence of soil–structure interaction (SSI) on the dynamic characteristics of buildings, a series of free-vibration experiments were performed on a 1/4-scale steel-frame structure. The structural fixed-base fundamental period was for the first time determined by experiments as to avoid evaluation errors in the conventional SSI analyses, and its numerical counterpart obtained by using SAP2000® was also given for comparison. A total of 34 scenarios, which varied with regard to overall stiffness and mass of the structure, were examined in the experiments and the numerical simulations. In each experimental scenario, the fundamental period of the structure was determined under fixed-base and flexible-base conditions. A newly proposed method by Luco using Dunkerley's formula to evaluate the lower bounds for structural natural frequencies considering SSI was validated by both experimental and numerical results. This method was found to exhibit excellent accuracy in predicting the fundamental period of the structure with SSI. This experimentally verified formula, having a broader application potential than the Jennings and Bielak and Veletsos and Meek expressions, could apply to a variety of researching areas in earthquake engineering and would be a useful reference for future seismic code revisions in assessing the basic period of the structure with SSI.

✉ Wei Xiong
bbbear2002@gmail.com

Li-Zhong Jiang
lzhjiang@csu.edu.cn

Yao-Zhuang Li
liyz@csu.edu.cn

[1]   School of Civil Engineering, Central South University, Changsha 410075, Hunan, China

[2]   National Engineering Laboratory of High-Rail Construction Technology, Central South University, Changsha 410075, Hunan, China

# 1 Introduction

The fundamental period is one of the most crucial indicators in evaluating the dynamic characteristics of a structure. In response spectrum-based methods, it is used to assess the base shear and deformation in a building, and therefore to determine the seismic force experienced by the building during ground shaking. Due to the ever-growing interest in performance-based seismic design, there is now an increasing awareness of the effect of soil–structure interaction (SSI) on the overall seismic resistant capacity of the structures. It is well known that there are differences between fundamental-mode parameters when considering SSI (flexible base) and not considering SSI (fixed base). Generally, SSI can lengthen the fundamental period and increase the overall damping of the system.

Numerous studies have examined the effects of SSI on the fundamental-model parameters of the SSI system. Khalil et al. (2007) investigated the influence of SSI on the fundamental period of buildings by finite-element modeling on one-story and multi-story buildings resting on flexible soil. They found that the soil–structure relative stiffness was the key factor governing fundamental period elongation induced by SSI. Kwon and Kim (2010) evaluated the formulas in ASCE 7-05 for steel and RC moment-resisting frames, shear wall buildings, braced frames, and other structural types by using over 800 basic periods from 191 buildings and 67 earthquakes, and they recommended to use $C_r$ factor 0.015 for shear-wall and other-type structures. Hatzigeorgiou and Kanapitsas (2013) analyzed 20 different real building configurations by detailed 3D finite-element modeling and modal eigenvalue evaluation, and summarized an empirical formula for assessing the fundamental period of reinforced concrete structures, which incorporated SSI effect. Zaicenco and Alkaz (2007) used finite-element method and bi-directional lumped-mass-story-stiffness numerical models for the study of SSI effect on an instrumented 16-story, reinforced concrete building in Moldova, and concluded that higher magnitude of ground excitation would enlarge SSI effect, that is, the natural period of the structure could be lengthened, and high frequencies of the basement be suppressed. Michel et al. (2011) quantified and modeled the relative frequency decay and damping variation of low-rise modern masonry buildings in order to bring an analytical method to encompass the basic frequency, in which they argued that the SSI phenomenon should also be accounted for. After examining and comparing the experimental results obtained by forced-vibration tests and that by finite-element analyses on a school building in Taiwan, Ko and Chen (2009) found that the flexibility of foundation had a considerable impact on the results of structural analysis. Trifunac et al. (2010) conducted a comprehensive study on the response of a 14-story reinforced concrete building in Srpska to 20-recorded earthquakes, and they found that essentially linear SSI was observed in these recorded data. Bhattacharya and Dutta (2004) performed a detailed parametric investigation of SSI on the lateral period of buildings with isolated and grid foundations by 3D finite-element analysis, in which variation-curve charts depending on dynamic properties were generalized for accurate assessment of SSI effect. Trifunac et al. (2001a, b) analyzed the amplitude and time-dependent variation of the fundamental period of a 7-story, reinforced concrete hotel building in Van Nuys, California. They concluded that changes in the fundamental period

of the building are mainly the result of nonlinear soil response. Stewart et al. (1999a, b) used system identification approaches to evaluate SSI for 77 strong motion data sets at 57 building sites, and found that the structure-to-soil relative stiffness influenced SSI most. Aviles (Avilés and Pérez-Rocha 1999, 2003, 2005; Avilés and Suárez 2002) performed systematic analytical surveys on the effects of SSI on the fundamental period and damping ratio of the structure.

In order to define SSI effect on the dynamic properties of a structure in the conventional field experiments or earthquake observations, researchers need to compute the structural characteristics with a fixed-base assumption via analytical/numerical models for comparison. However, the actual dynamic properties of the fixed-base structure might be much different from that obtained analytically/numerically. This is due to many reasons. Firstly, there may be discrepancies between the designed structure and the constructed structure. Secondly, the actual dimensions of the structural members, and the strength of the building materials etc. are inevitably more or less varied with that in design. And thirdly, the analytical/numerical models may not capture all the real characteristics of the building. As a result, the prediction accuracy of the structural fixed-base characteristics from analytical/ numerical calculation would be limited.

In this study, the dynamic properties of the fixed-base structure were directly measured from free-vibration experiments performed with the foundation tightly fastened on the reinforced concrete ground by anchor bolts. This could significantly reduce the error in the evaluation of fixed-base structural properties. The fixed-base fundamental periods acquired by using finite-element package SAP2000® were also presented for comparison.

This paper describes an experimental investigation of SSI on the fundamental-mode parameters of a 1/4-scale steel-frame model structure. This structure was designed so that adding/removing inter-story struts and weights could change the overall stiffness and weight. A total of 34 different scenarios with different structural stiffness and weight of the structure were examined in the experiments. Numerical simulations were also carried out for comparison. In each scenario, the fundamental period of the structure was determined under both fixed-base and flexible-base conditions.

Moreover, for the first time, the newly proposed method by Luco (2013) using Dunkerley's formula to evaluate the bounds for natural frequencies of the structure considering SSI was testified by both the experimental and numerical results obtained in this work. This method proposed by Luco has a broader application potential and preferable accuracy than the existing formulas for assessing the structural basic period with SSI, as evidenced both by the experimental and numerical results, rendering it a useful reference for future seismic code revisions. Limitations in this work were also given in the latter part of this paper. At last, conclusions concerning the SSI experiments and the analytical results were made.

## 2 Experimental setup and procedure

### 2.1 Model structure design

In the SSI experiments, a steel-frame structure model was constructed on a scale of 1/4, and a schematic view of which is presented in Fig. 1. Moving the slabs up/down within the four columns to 1.0 or 1.5 m can change the inter-story height of the structure. The dimensions of the structural members are presented in Table 1. The structural members
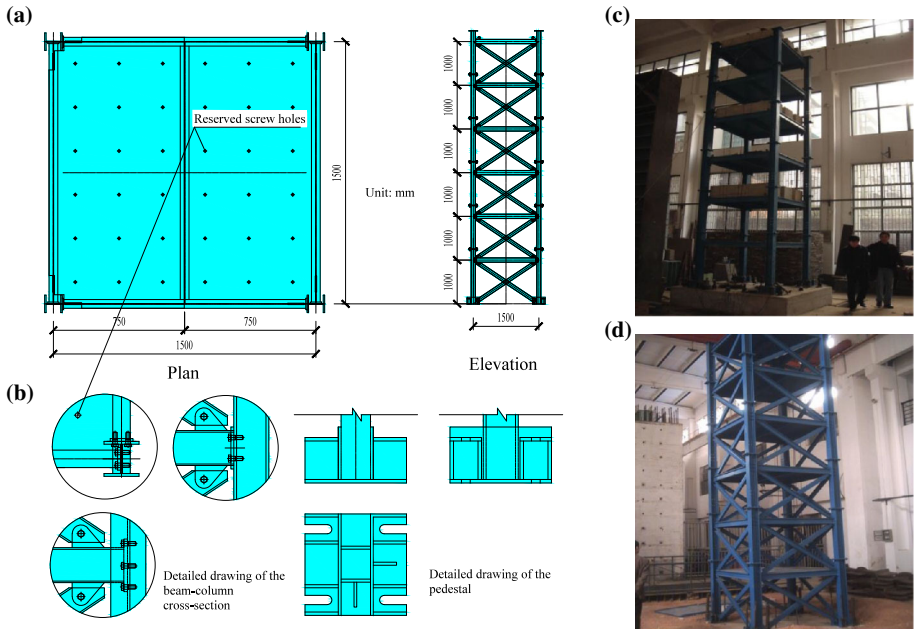
**Fig. 1** Schematic view and lay out of the steel-frame structure: **a** Plan and elevation view of the structure, **b** detailed drawings of the beam-column cross-section and the pedestal, **c** fixed-base structure, **d** flexible-base structure

**Table 1** Dimensions of the structural members (Unit: mm)

| Member | Column | Beam | Floor plate | Diagonal strut | Connection bolt | Steel grade |
|---|---|---|---|---|---|---|
| Dimension | H125 × 125 × 6.5 × 9 | H100 × 50 × 5 × 7 | Thickness = 10 | [8 (fixable)] | Grade 8.8 M12 | Q235 |

were connected using Grade 8.8 M12, high-strength, friction-grip bolts. Fitting or unfitting inter-story diagonal struts can change the overall stiffness of the building. Likewise, adding or removing additional weights can change the total mass of the structure. Each concrete-cast additional weight measures 300 mm × 350 mm × 1350 mm and weights 340.2 kg (the weight of the standard floor $m_s$ is 337.2 kg). The additional weights can be fixed on each floor of the structure through reserved screw holes on the floors. Initial findings can be found in the references (He et al. 2008; Shang et al. 2009).

Two identical square base mats, measuring 2000 mm × 2000 mm × 400 mm each, were used in the tests. One of the base mats was fixed on the concrete floor in the laboratory through anchor bolts to represent the fixed-base condition; the other was casted and formed in the soil excavation, which resembles the actual construction of the foundation, to represent the flexible-base condition. The base mat in the soil was fully embedded with an embed depth 400 mm, the thickness of the base mat.

## 2.2 Foundation soil

A reinforced-concrete soil container, measuring 32.5 m long × 6 m wide × 4 m deep, was constructed in the laboratory. The bottom of the soil container was directly connected to the natural soil deposit. 100 mm thick foam boards were set against the 4 inner walls of the soil box to absorb instant wave reflection during the tests. The backfill in the soil box was compacted in layers to resemble the natural deposit process. Each compaction was performed during a 1-m-depth interval, and in total five compactions were conducted. The natural density ($\rho$) of the bonded silica sand backfill is 1.64 g/cm$^3$, dry density 1.53 g/cm$^3$, and moisture capacity 7.2 %, and Poisson's ratio 0.3. Before the SSI experiments, borehole test was performed (Fig. 2) and the backfill shear-wave velocity was determined as 211 m/s.

## 2.3 Testing scheme

When the structure was assembled, the north–south (NS) direction was designated to be the strong axis, and the east–west (EW) direction the weak axis, due to the orientation of the H-section columns. The structure was instrumented with accelerometers, carefully installed to study its sway and rocking response. Two accelerometers in the NS and EW directions, respectively, were installed in the geometrical center of each floor to measure the structural sway components. Vertical accelerometers were installed at each end of the 4 margins of the base mat to record the rocking motion. The measure points in the NS, EW and vertical directions are illustrated in Fig. 3.

In the experiments, low-frequency sensitive transducers were used, considering that the fundamental frequency of the structure is within the low-frequency band. The transducers used in the experiments were of type 941B (Institute of Engineering Mechanics, China Seismology Bureau). Lower-band pass filter was applied to the sampled signals, and the frequency threshold was set to 30 Hz. Baseline corrections were also conducted using the Data Acquisition and Signal Processing (DASP) system offered by the China Seismology Bureau. According to the Nyquist–Shannon sampling



**Fig. 2** Velocity profile of the site with depth; the average velocity is 211 m/s
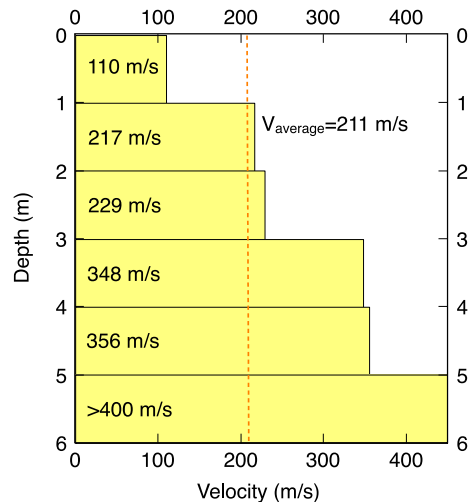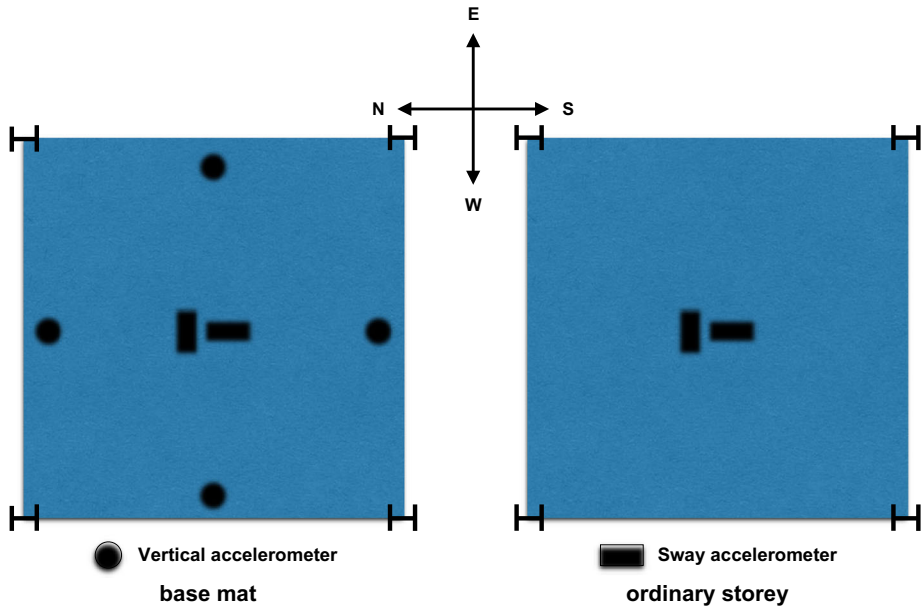
**Fig. 3** Locations of the accelerometers

principle, to avoid overlap, the sampling frequency must be two times the maximum frequency of the sampled signal. Thus the sampling rate was set to 256 Hz, and the duration 30 s.

In the SSI experiments, to change the overall stiffness and mass of the structure, the following variations were made:

- Inter-story height: 1.0, 1.5 m;
- Adding/removing additional weights: without weight, one order of weight, two orders of weights, three orders of weights;
- Adding/removing diagonal struts: without strut, struts in the odd-number stories, struts in the even-number stories, struts in all stories (in each story, two diagonal struts were installed in X shape).

A total of 34 scenarios were considered in the experiments. The influencing factors included the structure-to-soil relative stiffness, and the structure-to-soil mass ratio. The 34 scenarios can be divided into three groups: Group 1 (S1–S18) with no additional weight, the story height 1.0 m, and the struts varied; Group 2 (S19–S26) with no strut, the story height 1.0 m, and the additional weights varied; Group 3 (S27–S34) with no strut, the story height 1.5 m, and the additional weights varied. In Group 1 the structural stiffness variation was primarily focused, whereas in Group 2 and Group 3 the mass change. The detailed scenarios in the SSI experiments are given in Table 2. The structural stiffness $k$ is calculated by

$$k = \frac{4\pi^2}{T^2} \times m \tag{1}$$

**Table 2** Experimental scenarios

| Scenarios | Outline of the structural configuration | Direction | $k$ (N/m) | $k_n$ (N/m) | $m$ (kg) |
|---|---|---|---|---|---|
| Group 1: no additional weights; the story height 1.0 m; number of stories 6 | | | | | |
| S1 | Struts in all stories in the NS, EW directions | NS | 20,052,541.15 | 20,861,496.72 | 2596.7 |
| S2 | | EW | 16,936,446.94 | 20,625,442.08 | |
| S3 | Struts in odd stories in the NS, EW directions | NS | 8,841,324.142 | 8,120,564.667 | 2298.14 |
| S4 | | EW | 5,152,219.512 | 4,956,106.276 | |
| S5 | Struts in even stories in the NS, EW directions | NS | 9,313,263.668 | 7,470,901.573 | 2298.14 |
| S6 | | EW | 5,152,219.512 | 4,486,803.097 | |
| S7 | Struts in all stories in the NS direction, no struts in the EW direction | NS | 18,621,958.67 | 11,689,189.17 | 2298.14 |
| S8 | | EW | 894,370.2209 | 1,119,338.056 | |
| S9 | Struts in all stories in the EW direction, no struts in the NS direction | NS | 2,061,224.216 | 1,463,313.939 | 2298.14 |
| S10 | | EW | 15,748,988 | 17,356,398.35 | |
| S11 | Struts in odd stories in the NS direction, no struts in the EW direction | NS | 8,202,116.58 | 7,996,379.448 | 2148.86 |
| S12 | | EW | 882,194.4296 | 1,134,934.566 | |
| S13 | Struts in even stories in the NS direction, no struts in the EW direction | NS | 8,815,152.48 | 7,550,159.27 | 2148.86 |
| S14 | | EW | 857,682.4905 | 1,103,235.186 | |
| S15 | Struts in odd stories in the EW direction, no struts in the NS direction | NS | 2,026,546.554 | 1,483,913.861 | 2148.86 |
| S16 | | EW | 5,035,220.094 | 5,113,710.261 | |
| S17 | Struts in even stories in the EW direction, no struts in the NS direction | NS | 1,970,296.753 | 1,436,664.288 | 2148.86 |
| S18 | | EW | 5,035,220.094 | 4,546,387.458 | |
| Group 2: no diagonal struts; the story height 1.0 m; number of stories 6 | | | | | |
| S19 | No additional weight | NS | 1,856,612.133 | 1,793,442.835 | 1999.58 |
| S20 | | EW | 824,627.6399 | 819,322.8763 | |
| S21 | One order of additional weights | NS | 1,984,809.369 | 1,921,933.741 | 4040.78 |
| S22 | | EW | 858,757.1925 | 878,621.567 | |
| S23 | Two orders of additional weights | NS | 2,630,893.446 | 2,480,873.884 | 6081.98 |
| S24 | | EW | 1,114,760.503 | 1,140,167.334 | |
| S25 | Three orders of additional weights | NS | 2,371,911.818 | 2,286,557.645 | 8123.18 |
| S26 | | EW | 1,161,731.223 | 1,048,282.852 | |
| Group 3: no diagonal struts; the story height 1.5 m; number of stories 4 | | | | | |
| S27 | No additional weight | NS | 1,230,133.934 | 1,295,605.055 | 1491.72 |
| S28 | | EW | 459,495.2022 | 413,688.4769 | |
| S29 | One order of additional weights | NS | 1,314,446.684 | 1,279,243.819 | 2852.52 |
| S30 | | EW | 484,321.7891 | 423,935.3106 | |
| S31 | Two orders of additional weights | NS | 1,420,268.821 | 1,422,762.343 | 4212.8 |
| S32 | | EW | 545,230.9207 | 472,159.9184 | |
| S33 | Three orders of additional weights | NS | 1,382,954.728 | 1,509,607.997 | 5574.12 |
| S34 | | EW | 521,006.2846 | 502,134.495 | |
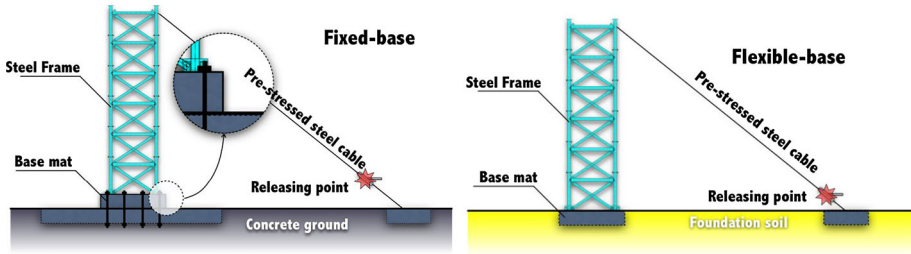
**Fig. 4** Diagrams of free-vibration tests for structures with a fixed base and a flexible base

In which $T$ denotes the fixed-base fundamental period of the structure either measured from the SSI experiments or from the numerical calculations by using SAP2000®. The letter $m$ is the total mass of the structure.

## 2.4 Testing method

The free-vibration testing method was used in the SSI experiments, which consisted of forcing the structure into free-vibration via suddenly releasing a pre-stressed steel cable anchored between the building roof and the nearby ground surface in the two orthogonal directions (EW and NS) (Fig. 4). The initial displacement of the roof that forced the structure to oscillate was limited to 3 mm. The testing procedure consisted of two stages. In the first stage, the base of the structure was fixed on stiff reinforced concrete grounds
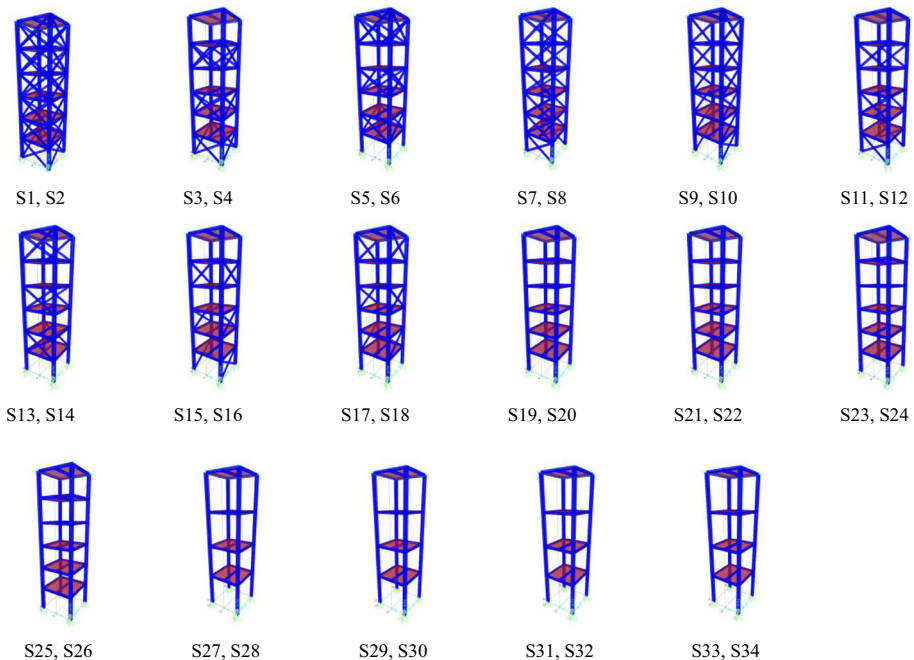


**Fig. 5** Schematic views of the scenarios in the numerical simulation using SAP2000®

**Table 3** Data obtained by the SSI experiments and by the numerical simulations using SAP2000®

| Scenarios | Direction | Experiment | | SAP2000 | |
|---|---|---|---|---|---|
| | | Fixed-base condition fundamental period $T$ | Flexible-base condition fundamental period $T_1$ | Fixed-base condition fundamental period $T_n$ | $T_1/T$ |
| Group 1 | | | | | |
| S1 | NS | 0.0715 | 0.0899 | 0.0701 | 1.2573 |
| S2 | EW | 0.0778 | 0.0989 | 0.0705 | 1.2712 |
| S3 | NS | 0.1013 | 0.1137 | 0.1057 | 1.1224 |
| S4 | EW | 0.1327 | 0.1524 | 0.1353 | 1.1485 |
| S5 | NS | 0.0987 | 0.1192 | 0.1102 | 1.2077 |
| S6 | EW | 0.1327 | 0.1485 | 0.1422 | 1.1191 |
| S7 | NS | 0.0698 | 0.0995 | 0.0881 | 1.4255 |
| S8 | EW | 0.3185 | 0.3512 | 0.2847 | 1.1027 |
| S9 | NS | 0.2098 | 0.2314 | 0.249 | 1.1030 |
| S10 | EW | 0.0759 | 0.0983 | 0.0723 | 1.2951 |
| S11 | NS | 0.1017 | 0.1129 | 0.103 | 1.1101 |
| S12 | EW | 0.3101 | 0.3415 | 0.2734 | 1.1013 |
| S13 | NS | 0.0981 | 0.1199 | 0.106 | 1.2222 |
| S14 | EW | 0.3145 | 0.3469 | 0.2773 | 1.1030 |
| S15 | NS | 0.2046 | 0.2230 | 0.2391 | 1.0899 |
| S16 | EW | 0.1298 | 0.1516 | 0.1288 | 1.1680 |
| S17 | NS | 0.2075 | 0.2270 | 0.243 | 1.0940 |
| S18 | EW | 0.1298 | 0.1486 | 0.1366 | 1.1448 |
| Group 2 | | | | | |
| S19 | NS | 0.2062 | 0.2210 | 0.2098 | 1.0718 |
| S20 | EW | 0.3094 | 0.3417 | 0.3104 | 1.1044 |
| S21 | NS | 0.2835 | 0.3040 | 0.2881 | 1.0723 |
| S22 | EW | 0.4310 | 0.4702 | 0.4261 | 1.0910 |
| S23 | NS | 0.3021 | 0.3691 | 0.3111 | 1.2218 |
| S24 | EW | 0.4641 | 0.5713 | 0.4589 | 1.2310 |
| S25 | NS | 0.3677 | 0.4241 | 0.3745 | 1.1534 |
| S26 | EW | 0.5254 | 0.6571 | 0.5531 | 1.2507 |
| Group 3 | | | | | |
| S27 | NS | 0.2188 | 0.2597 | 0.2132 | 1.1869 |
| S28 | EW | 0.3580 | 0.3932 | 0.3773 | 1.0983 |
| S29 | NS | 0.2927 | 0.3522 | 0.2967 | 1.2033 |
| S30 | EW | 0.4822 | 0.5681 | 0.5154 | 1.1781 |
| S31 | NS | 0.3422 | 0.4184 | 0.3419 | 1.2227 |
| S32 | EW | 0.5523 | 0.6458 | 0.5935 | 1.1693 |
| S33 | NS | 0.3989 | 0.4813 | 0.3818 | 1.2066 |
| S34 | EW | 0.6499 | 0.7423 | 0.662 | 1.1422 |

(fixed-base condition). In the second stage, the foundation was placed on flexible soil in the soil box (flexible-base condition). The fundamental period and basic mode were determined in these two stages (Table 3).

# 3 Numerical simulations by using SAP2000<sup>®</sup>

The fixed-base fundamental period was also obtained by numerical simulation using SAP2000<sup>®</sup> for comparison. The modeling of the steel frame was strictly in line with the standard process in the engineering finite-element simulation. A schematic view of these models is presented in Fig. 5, and the obtained fixed-base fundamental periods are given in Table 3.

# 4 Experimental and numerical results

## 4.1 Fundamental period

Power spectral density (PSD) technique was used to extract the fundamental period of the structure from the collected experimental data under different scenarios. This method is designed to encompass the fundamental period of a linear and time-invariant system. In all of the scenarios, with either a fixed or flexible base, the fundamental period can be obtained by PSD on the roof acceleration time-history. Some typical roof acceleration time-histories of the structure with/without base flexibility are shown in Fig. 6, while the PSDs of the selected scenarios are shown in Fig. 7. The period lengthening ratio can be defined as:

$$\text{Period lengthening ratio } = \frac{T_1}{T} \tag{2}$$

where $T_1$ and $T$ represent the flexible-base fundamental period and the fixed-base fundamental period of the structure, respectively. The fundamental periods extracted from the experimental data and from the numerical modeling are given in Table 3. The fundamental periods by PSD on acceleration time-histories of other stories were found in agreement
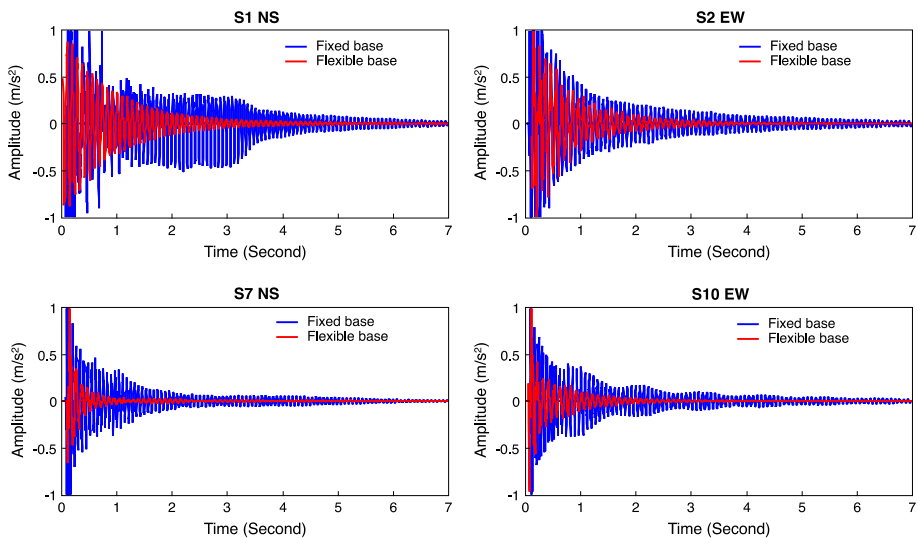


**Fig. 6** Normalized typical roof acceleration time histories of the structure with fixed-base or flexible-base condition
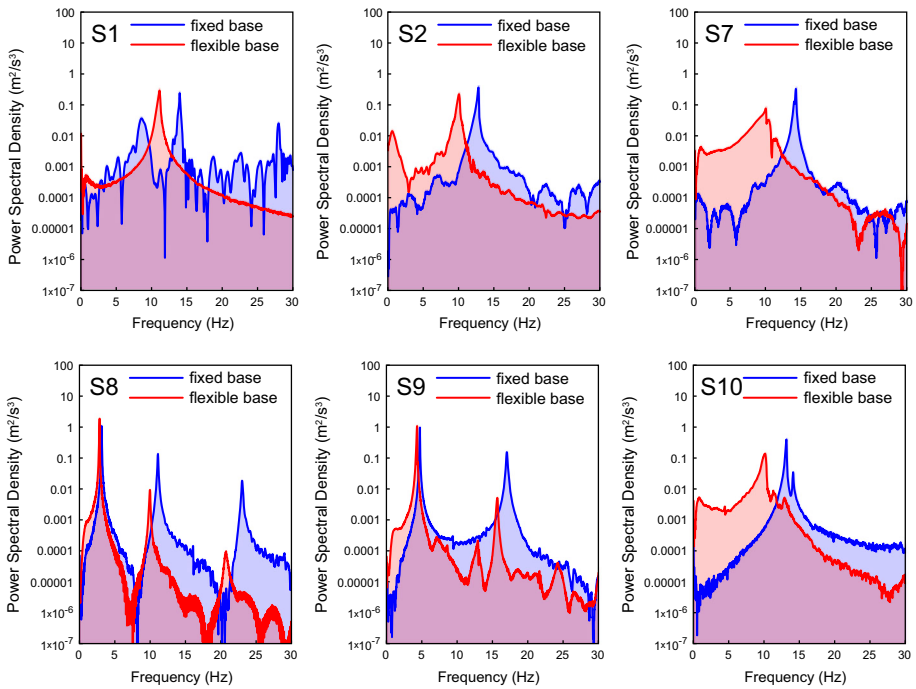
**Fig. 7** Power spectral density (PSD) of the roof acceleration time-history of the structure with/without foundation flexibility, only selected scenarios are included

with that obtained on the roof. Therefore the consistency and accuracy of the PSD method for extracting the fundamental period of the structure could be guaranteed.

As shown in Fig. 7 and Table 3, for the same scenario, the fundamental period of the structure with a flexible base was greater than that with fixed base, which represents the SSI effect. The vibration amplitude in flexible-base case attenuates faster with time than that in fixed-base case (Fig. 6), which shows that the damping ratio of the structure was increased with foundation flexibility.

The structure-to-soil relative stiffness could be considered as the factor that most strongly influences the period lengthening of the soil–structure system (Table 3). The structure became stiffer when installed more diagonal struts. The period lengthening ratio $T_1/T$ increased with increasing installed diagonal struts in either the EW or NS direction. For example, in S1 and S2, struts were fixed in all stories in the NS and EW directions (Maximum stiffness in both directions). The period lengthening ratios were 1.2564 (NS direction) and 1.2722 (EW direction). The structural stiffness is greater in test S1 than in S2, while the period elongation in S1 is smaller than in S2. This may stem from the inhomogeneity of the soil. The soil may be compacted stiffer along the NS direction, and softer along the EW direction. Consequently the structure-to-soil relative stiffness is greater in the EW direction than in the NS direction. In S7 and S8, struts were fixed in all stories in the NS direction, while no strut in the EW direction. The period lengthening ratios were 1.4245 (NS direction) and 1.1026 (EW direction). In contrast to S7 and S8, in S9 and S10, the structural stiffness was maximized in the EW direction (all struts were installed), and minimized in the NS direction (no strut was installed). Accordingly, the

period lengthening ratio in the EW direction (1.2954) was much greater than that in the NS direction (1.1030). In S19 and S20, where both directions had minimum structural stiffness, i.e. no struts installed, the period lengthening ratios were 1.0720 (NS direction) and 1.1044 (EW direction).

The increase of period lengthening ratio $T_1/T$ with structure-to-soil mass ratio is not as evident as that with structure-to-soil relative stiffness. In Group 2, $T_1/T$ accords to 1.0718 (S19, no weight), 1.0723 (S21, one order of weight), 1.2218 (S23, two orders of weights), 1.1534 (S25, three orders of weights) in NS direction. As for S20, S22, S24 and S26 in EW direction, $T_1/T$ accords to 1.1044, 1.0910, 1.2310 and 1.2517 respectively, which shows a clearer trend of increase with mass ratio than that in NS direction. For Group 3, $T_1/T$ are 1.1869 (S27), 1.2033 (S29), 1.2227 (S31) and 1.2066 (S33) in NS direction; in EW direction, $T_1/T$ are 1.0983 (S28), 1.1781 (S30), 1.1693 (S32) and 1.1422 (S34). The increase of $T_1/T$ with mass ratio is not evident in Group 3.

The experimentally obtained fixed-base fundamental periods are compared to that using the formulas recommended by ASCE 7-05 (2005). A well-established and comprehensive summary of the code-based formulas for evaluating the lower bound of the structural basic period was given by Kwon and Kim (2010). In the scenarios, S1–S18 represents the concentrally braced frame (CBF), and S19–S34 represents the moment resisting frame (MRF). This comparison is illustrated in Fig. 8. The empirical formula recommended by ASCE 7-05 for assessing the lower-bound structural basic period is:
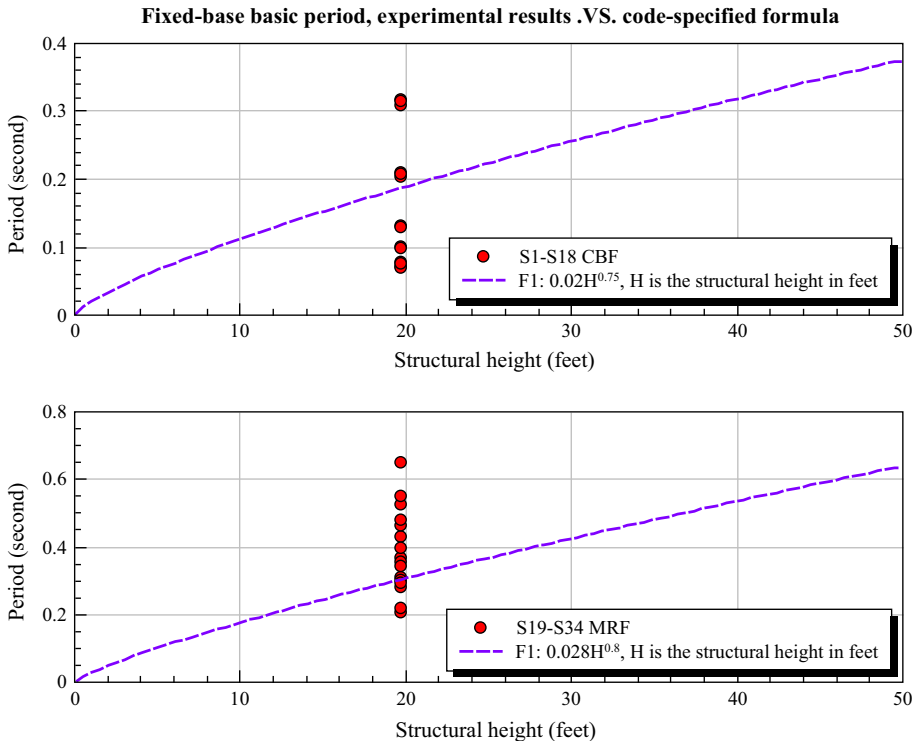


**Fig. 8** Basic periods obtained by experiments versus that by empirical formula recommended by ASCE 7-05

$$T_a = C_r H^x \tag{3}$$

In which $T_a$ denotes the evaluated basic period, $H$ the overall structural height in feet, and $C_r$ and $x$ coefficients. For CBF, the coefficients are $C_r = 0.02$, $x = 0.75$. For MRF, the coefficients are $C_r = 0.028$, $x = 0.8$. It is noteworthy that the overall height of the structure in all the scenarios was kept constant and not changed. As shown in Fig. 8, the code-specified formula may not be adequate for evaluating the fundamental period of the structure due to its simplicity. The empirical formula only takes one variable ($H$) into account, reflecting the change in structural height, but have neglected the complexity within the structure, such as bracing configuration, inter-story height, load capacity, and so on. More proper would be to calculate the fixed-base structural basic period analytically or numerically (e.g. via SAP2000 package), and then to calibrate it by the revised Dunkerley's formula. By this procedure perceivably more accurate predictions could be achieved.

The fixed-base fundamental periods $T_n$ obtained by numerical simulations using SAP2000 were also presented in Table 3. As shown, the discrepancies between $T$ and $T_n$ are noticeable but not prominent. In Sect. 5 both $T$ and $T_n$ will be used in calculating the flexible-base fundamental period.

### 4.2 Fundamental mode shape

The fundamental mode shape of the structure can be obtained from the response ratio at different measurement points in the fundamental period (Fig. 9). The fundamental mode shape of the structure with base flexibility was different from that with a fixed base. If SSI is considered, the base mat exhibits both sway and rocking motion, which would hence change the overall fundamental mode shape of the structure. Moreover, in the basic mode, the foundation and roof were in-phase, that the foundation swaying plus rocking would increase the amplitude of each storey. As a result, the structural basic mode would be changed. Figure 10 illustrates the modal displacement amplitudes of the base mat with $1/\sigma$ in different scenarios. As shown, the modal displacement amplitude of the base mat $d1$ increases with increasing $1/\sigma$ (Table 4).

The structure-to-soil relative stiffness $1/\sigma$ is defined by

$$\frac{1}{\sigma} = \frac{h}{V_s T} \tag{4}$$

In which $\sigma$ represents the soil-to-structure relative stiffness, $V_s$ the shear wave velocity of the site, $h$ the height of the structure. The relation between $1/\sigma$ and $d1$ (generalized
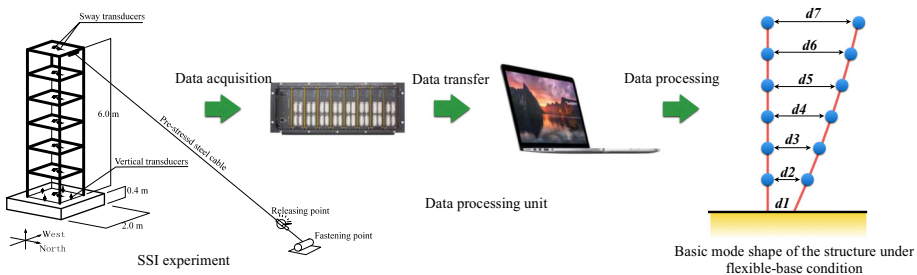


**Fig. 9** Base mode shape of the structure under flexible-base condition

**Fig. 10** The base displacement of the fundamental mode shape versus structure-to-soil relative stiffness $1/\sigma$, the definition of $d1$ can be found in Fig. 9, scenarios in Group 1 were included in this figure
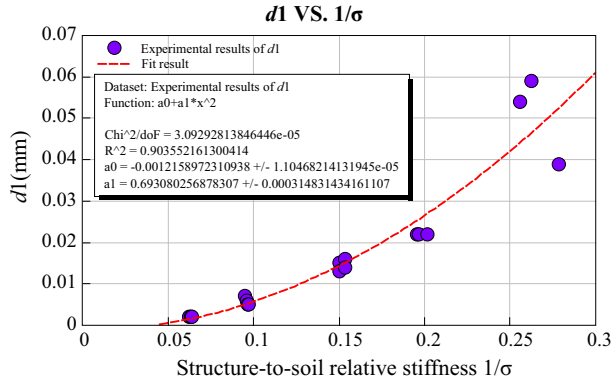


**Table 4** Fundamental mode shape of the structure incorporating foundation flexibility

| Story | S1 | S2 | S3 | S4 | S5 | S6 | S7 | S8 | S9 | S10 |
|-------|-------|-------|-------|-------|-------|-------|-------|-------|-------|-------|
| $d7$ | 1.000 | 1.000 | 1.000 | 1.000 | 1.000 | 1.000 | 1.000 | 1.000 | 1.000 | 1.000 |
| $d6$ | 0.851 | 0.861 | 0.841 | 0.862 | 0.941 | 0.923 | 0.889 | 0.757 | 0.865 | 0.942 |
| $d5$ | 0.723 | 0.691 | 0.793 | 0.753 | 0.741 | 0.71 | 0.702 | 0.662 | 0.743 | 0.793 |
| $d4$ | 0.542 | 0.57 | 0.502 | 0.541 | 0.620 | 0.601 | 0.488 | 0.499 | 0.532 | 0.581 |
| $d3$ | 0.384 | 0.388 | 0.438 | 0.465 | 0.311 | 0.376 | 0.273 | 0.231 | 0.393 | 0.371 |
| $d2$ | 0.204 | 0.133 | 0.084 | 0.093 | 0.211 | 0.167 | 0.083 | 0.114 | 0.207 | 0.193 |
| $d1$ | 0.054 | 0.039 | 0.013 | 0.022 | 0.015 | 0.022 | 0.002 | 0.022 | 0.059 | 0.007 |
| Story | S11 | S12 | S13 | S14 | S15 | S16 | S17 | S18 | S19 | S20 |
| $d7$ | 1.000 | 1.000 | 1.000 | 1.000 | 1.000 | 1.000 | 1.000 | 1.000 | 1.000 | 1.000 |
| $d6$ | 0.887 | 0.845 | 0.886 | 0.867 | 0.840 | 0.891 | 0.953 | 0.911 | 0.896 | 0.858 |
| $d5$ | 0.714 | 0.733 | 0.703 | 0.680 | 0.789 | 0.710 | 0.762 | 0.726 | 0.718 | 0.714 |
| $d4$ | 0.491 | 0.528 | 0.485 | 0.485 | 0.490 | 0.516 | 0.640 | 0.529 | 0.491 | 0.520 |
| $d3$ | 0.276 | 0.451 | 0.270 | 0.281 | 0.431 | 0.355 | 0.330 | 0.335 | 0.273 | 0.328 |
| $d2$ | 0.083 | 0.090 | 0.082 | 0.085 | 0.085 | 0.165 | 0.213 | 0.167 | 0.116 | 0.161 |
| $d1$ | 0.002 | 0.022 | 0.002 | 0.003 | 0.014 | 0.005 | 0.016 | 0.006 | 0.002 | 0.005 |

displacement of the base mat in the fundamental mode shape of the structure, see Fig. 9) is expressed by

$$d1 = 0.693(1/\sigma)^2 - 0.00121 \tag{5}$$

The confidence intervals of the regression curve are presented in Fig. 10. It is noted that there is much more uncertainty of the prediction formula in the range $1/\sigma > 0.25$. This may due to data collection error of $d1$ when $1/\sigma$ is $>0.25$, yet Eq. (5) may generally capable of predicting the increase trend of $d1$ with $1/\sigma$ with a moderate confidence.

## 5 Analyses

In order to determine the fundamental period of a structure incorporating SSI, several authors have made many fruitful works, including early studies conducted by Veletsos and Meek (1974), Veletsos and Nair (1975) and Bielak (1974). In a recent research, Luco (2013) proposed a new expression using Dunkerley's formula and then obtained an improved estimate. This improved estimate could cover a wide spectrum of possible SSI problems with satisfactory predicting accuracy. In this work, this formula was for the first time applied to evaluate the lower bound of the fundamental period of the structure considering base flexibility.

### 5.1 Analyses procedures

A simplified SSI analytical model is introduced in order to quantify the effect of SSI on the fundamental period of the structure (Fig. 11). This equivalent model was widely used to represent the dynamic SSI problem (Kausel 2010; Tileylioglu et al. 2011). It includes a single DOF structure with height $h$ resting on a flexible base, which is represented by the frequency-related, complex-valued sway impedance $k_{uu}$ and rocking impedance $k_{\theta\theta}$. This can be viewed as the direct modeling of a one-story building, and more generally, an approximation for the multi-story structure dominated by its basic mode. The fundamental period can be viewed as the flexible-base fundamental-mode parameter, since it represents the dynamic response of the structure with sway and rocking motions.

The mass matrix $[\mathbf{M}]$ and stiffness matrix $[\mathbf{K}]$ of this simplified model are

$$[\mathbf{M}] = \begin{bmatrix} m & m & mh \\ m & m + m_0 & mh \\ mh & mh & I + I_0 + mh^2 \end{bmatrix}, \quad [\mathbf{K}] = \begin{bmatrix} k & 0 & 0 \\ 0 & k_{uu} & k_{u\theta} \\ 0 & k_{\theta u} & k_{\theta\theta} \end{bmatrix} \quad (6)$$

In which $m$ denotes the mass of the structure, $I$ the mass moment of inertia of the structure, $m_0$ the mass of the rigid foundation, $I_0$ the mass moment of inertia of the rigid
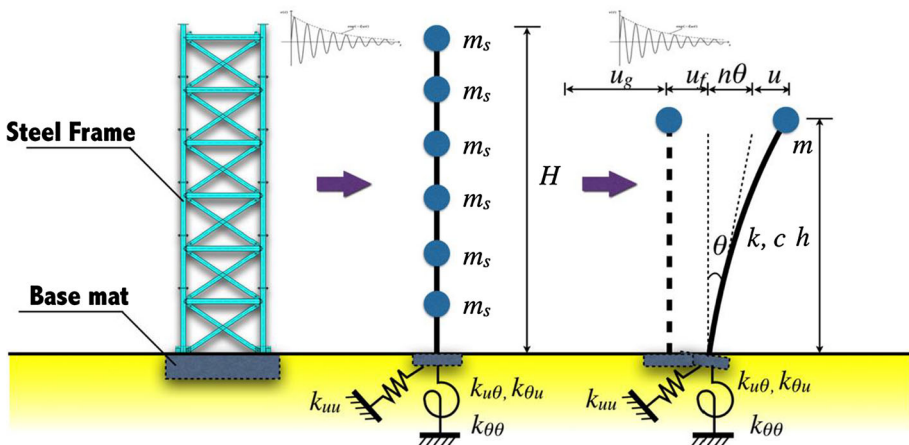


**Fig. 11** The simplified one-DOF SSI model

foundation, $h$ the height of the single-DOF structure, $k$ the lateral stiffness of the structure, and $k_{uu}$, $k_{\theta\theta}$, $k_{u\theta} = k_{\theta u}$ respectively the sway, rocking, and coupling impedances of the rigid foundation embedded in the flexible soil. The determination of foundational impedances has been a heated research topic among the earthquake engineering communities over the past 30 years, of which multiple fruitful works are achieved (Kausel 2010; Tileylioglu et al. 2011). The impedance expression by Gazetas (1991) was adopted in this analysis, because it presents a complete set of simple formulas covering nearly all foundation base shapes and different embed types. These formulas are very handy and straightforward for engineering practice, giving a comprehensive summary of previous well-established formulas for calculating foundation impedance. For computational simplicity, the frequency dependency of the compliance coefficients is ignored and the static stiffness is used in the analysis. The impedance functions are expressed by (Gazetas 1991):

$$
\begin{aligned}
K_{u,emb} &= K_{u,surface}\Big[1 + 0.15(D/B)^{0.5}\Big]\Big\{1 + 0.52\big[(d/B)\big(A_w/L^2\big)\big]^{0.4}\Big\} \\
K_{\theta,emb} &= K_{\theta,surface}\Big\{1 + 1.26(d/B)\Big[1 + (d/B)(d/D)^{-0.2}(B/L)^{0.5}\Big]\Big\} \\
K_{u\theta} &\approx (1/3)dK_{u,emb}
\end{aligned}
\tag{7}
$$

where

$$
\begin{aligned}
K_{u,surface} &= [2GL/(2-\upsilon)]\big(2 + 2.50\chi^{0.85}\big) \text{ with } \chi = A_b/4L^2 \\
K_{\theta,surface} &= [G/(1-\upsilon)]I^{0.75}(L/B)^{0.25}[2.4 + 0.5(B/L)]
\end{aligned}
\tag{8}
$$

where $K$ denotes the static impedance of the foundation. The subscripts ($u$ and $\theta$) represent swaying and rocking motion of the foundation, respectively. The subscript $emb$ and $surface$ represent the embedded and surface foundation, respectively. The italicized letter $G$ denotes the shear modulus of the soil, expressed by

$$
G = \rho V_s^2
\tag{9}
$$

where $\rho$ and $V_s$ represent the natural density and the equivalent shear-wave velocity of the soil, respectively. The letter $D$ represents foundation embed depth, $B$ half width of the foundation, $d$ foundation contact depth, $A_w$ total sidewall contact area, $L$ half length of the foundation, $\upsilon$ Poisson ratio, $A_b$ total base contact area, $I$ Area moment of inertia of the basement. It is assumed that the foundation sidewalls are in full contact with the soil, that is, $D = d$, $B = L$, $A_w = 2DB$, $A_b = 4BL$ to conform to the actual fact. The coefficients are listed in Table 5.

The coefficients necessary to determine the smallest eigenvalue $\lambda_1 = \omega_1^2 = (2\pi/T_1)^2$ yield (Luco 2013):

$$
|\mathbf{M}| = m_0 m(I_0 + I)
\tag{10}
$$

Table 5  Coefficients for Gazetas (1991) formula

| $B$ | $D$ | $A_w$ | $A_b$ | $\upsilon$ | $\rho$ | $V_s$ |
|---|---|---|---|---|---|---|
| 1.0 m | 0.4 m | 2.0 m$^2$ | 4.0 m$^2$ | 0.3 | 1.64 g/cm$^3$ | 211 m/s |

$$\alpha_3 = \frac{|\mathbf{K}|}{|\mathbf{M}|} = \frac{k(k_{uu}k_{\theta\theta} - k_{u\theta}k_{\theta u})}{m_0 m (I_0 + I)} \tag{11}$$

$$\alpha_2 = \frac{1}{|\mathbf{M}|} \left( \begin{vmatrix} m & 0 & 0 \\ m & k_{uu} & k_{u\theta} \\ mh & k_{\theta u} & k_{\theta\theta} \end{vmatrix} + \begin{vmatrix} k & m & 0 \\ 0 & m+m_0 & k_{u\theta} \\ 0 & mh & k_{\theta\theta} \end{vmatrix} + \begin{vmatrix} k & 0 & mh \\ 0 & k_{uu} & mh \\ 0 & k_{\theta u} & I+I_0+mh^2 \end{vmatrix} \right)$$

$$= \frac{m(k_{uu}k_{\theta\theta} - k_{u\theta}k_{\theta u}) + k[(m+m_0)k_{\theta\theta} - mhk_{u\theta}] + k[(I+I_0+mh^2)k_{uu} - mhk_{\theta u}]}{m_0 m (I_0 + I)} \tag{12}$$

$$\alpha_1 = \frac{1}{|\mathbf{M}|} \left( \begin{vmatrix} k & m & mh \\ 0 & m+m_0 & mh \\ 0 & mh & I+I_0+mh^2 \end{vmatrix} + \begin{vmatrix} m & 0 & mh \\ m & k_{uu} & mh \\ mh & k_{\theta u} & I+I_0+mh^2 \end{vmatrix} + \begin{vmatrix} m & m & 0 \\ m & m+m_0 & k_{u\theta} \\ mh & mh & k_{\theta\theta} \end{vmatrix} \right)$$

$$= \frac{k[(m+m_0)(I+I_0) + h^2 m_0 m] + k_{uu}m(I+I_0) + k_{\theta\theta}m_0 m}{m_0 m (I_0 + I)} \tag{13}$$

Then the fundamental period of the structure considering SSI effect can be expressed by

$$T_1 = \frac{2\pi}{\omega_1} = 2\pi\sqrt{\frac{1}{\lambda_1}} = 2\pi\sqrt{\frac{1}{2}\left(\frac{\alpha_2}{\alpha_3}\right) + \frac{1}{2}\sqrt{\left(\frac{\alpha_2}{\alpha_3}\right)^2 - 4\frac{\alpha_1}{\alpha_3}}} \tag{14}$$

## 5.2 Results

The estimated fundamental periods of the structure with SSI in different scenarios, compared to those determined in the experiments, are presented in Table 6. The discrepancy $D_0/D_n$ between the flexible-base fundamental period obtained experimentally ($T_1$) and that by numerical simulation ($T_{1p}/T_{1pn}$) are given as follow:

$$\begin{aligned} D_0 &= (T_1 - T_{1p})/T_1 \\ D_n &= (T_1 - T_{1pn})/T_1 \end{aligned} \tag{15}$$

Figure 12 presents the comparison between the measured fundamental periods of the structure with SSI and that obtained analytically. Both results acquired from fixed-base fundamental periods by experiments ($T_{1p}$) and those by SAP2000 simulations ($T_{1pn}$) are presented in this figure. As shown, it can be noted that generally the results are in excellent agreement with each other, indicating that the Dunkerley's improved estimate proposed by Luco (2013) can satisfactorily predict the basic period of the structure incorporating SSI. For sub-figure group a, the discrepancies of the results in Group 2 (0.11) and Group 3 (0.139) are greater than that in Group 1 (0.072) in Table 6. This may stem from the nonlinear response of the structure invoked by the additional weights. Since one order weight of the structure, or more orders of weights were added, the structure might 'yield' to some extent during the oscillation, which might introduce certain degree of structural nonlinearity, yet the response of the superstructure in all scenarios were mainly in the elastic range due to the small amount of the initial input energy, which was evidenced by a bunch of

Table 6 Fundamental period of the structure incorporating SSI, obtained by experiments versus that by theoretical calculation

| Scenarios | Direction | Fundamental period $T_1$ obtained by experiments | Fundamental period $T_{lp}$ obtained by theoretical calculation using $T$ | Fundamental period $T_{lpn}$ obtained by theoretical calculation using $T_n$ | $D_0$ | $D_{average}$ | Total $D_{average}$ | $D_n$ | $D_{n\ -\ average}$ | Total $D_{n\ -\ average}$ |
|---|---|---|---|---|---|---|---|---|---|---|
| Group 1 | | | | | | | | | | |
| S1 | NS | 0.0899 | 0.0873 | 0.0862 | 0.029 | 0.0717 | 0.097 | 0.0412 | 0.0426 | 0.0743 |
| S2 | EW | 0.0989 | 0.0925 | 0.0865 | 0.065 | | | 0.1254 | | |
| S3 | NS | 0.1137 | 0.1117 | 0.1157 | 0.018 | | | −0.0176 | | |
| S4 | EW | 0.1524 | 0.1408 | 0.1432 | 0.076 | | | 0.0604 | | |
| S5 | NS | 0.1192 | 0.1093 | 0.1198 | 0.083 | | | −0.0050 | | |
| S6 | EW | 0.1485 | 0.1408 | 0.1498 | 0.052 | | | −0.0088 | | |
| S7 | NS | 0.0995 | 0.0842 | 0.0999 | 0.154 | | | −0.0040 | | |
| S8 | EW | 0.3512 | 0.3219 | 0.2885 | 0.083 | | | 0.1785 | | |
| S9 | NS | 0.2314 | 0.2150 | 0.2534 | 0.071 | | | −0.0951 | | |
| S10 | EW | 0.0983 | 0.0893 | 0.0863 | 0.092 | | | 0.1221 | | |
| S11 | NS | 0.1129 | 0.1114 | 0.1126 | 0.013 | | | 0.0027 | | |
| S12 | EW | 0.3415 | 0.3134 | 0.2771 | 0.082 | | | 0.1886 | | |
| S13 | NS | 0.1199 | 0.1081 | 0.1153 | 0.098 | | | 0.0384 | | |
| S14 | EW | 0.3469 | 0.3178 | 0.2810 | 0.084 | | | 0.1900 | | |
| S15 | NS | 0.2230 | 0.2096 | 0.2434 | 0.060 | | | −0.0915 | | |
| S16 | EW | 0.1516 | 0.1375 | 0.1366 | 0.093 | | | 0.0989 | | |
| S17 | NS | 0.2270 | 0.2124 | 0.2472 | 0.064 | | | −0.0890 | | |
| S18 | EW | 0.1486 | 0.1375 | 0.1440 | 0.075 | | | 0.0310 | | |
| Group 2 | | | | | | | | | | |
| S19 | NS | 0.2210 | 0.2108 | 0.2143 | 0.046 | 0.11 | | 0.0303 | 0.0983 | |
| S20 | EW | 0.3417 | 0.3125 | 0.3135 | 0.085 | | | 0.0825 | | |
| S21 | NS | 0.3040 | 0.2902 | 0.2947 | 0.045 | | | 0.0306 | | |
| S22 | EW | 0.4702 | 0.4355 | 0.4306 | 0.074 | | | 0.0842 | | |

**Table 6** continued

| Scenarios | Direction | Fundamental period $T_1$ obtained by experiments | Fundamental period $T_{1p}$ obtained by theoretical calculation using $T$ | Fundamental period $T_{1pn}$ obtained by theoretical calculation using $T_n$ | $D_0$ | $D_{average}$ | Total $D_{average}$ | $D_n$ | $D_{n-average}$ | Total $D_{n-average}$ |
|---|---|---|---|---|---|---|---|---|---|---|
| S23 | NS | 0.3691 | 0.3116 | 0.3203 | 0.156 | | | 0.1322 | | |
| S24 | EW | 0.5713 | 0.4703 | 0.4652 | 0.177 | | | 0.1857 | | |
| S25 | NS | 0.4241 | 0.3781 | 0.3847 | 0.108 | | | 0.0929 | | |
| S26 | EW | 0.6571 | 0.5327 | 0.5601 | 0.189 | | | 0.1476 | | |
| Group 3 | | | | | | | | | | |
| S27 | NS | 0.2597 | 0.2220 | 0.2165 | 0.145 | 0.139 | | 0.1663 | 0.1216 | |
| S28 | EW | 0.3932 | 0.3600 | 0.3792 | 0.084 | | | 0.0356 | | |
| S29 | NS | 0.3522 | 0.2973 | 0.3013 | 0.156 | | | 0.1445 | | |
| S30 | EW | 0.5681 | 0.4850 | 0.5180 | 0.146 | | | 0.0882 | | |
| S31 | NS | 0.4184 | 0.3480 | 0.3477 | 0.168 | | | 0.1690 | | |
| S32 | EW | 0.6458 | 0.5559 | 0.5969 | 0.139 | | | 0.0757 | | |
| S33 | NS | 0.4813 | 0.4055 | 0.3887 | 0.157 | | | 0.1924 | | |
| S34 | EW | 0.7423 | 0.6540 | 0.6670 | 0.119 | | | 0.1014 | | |
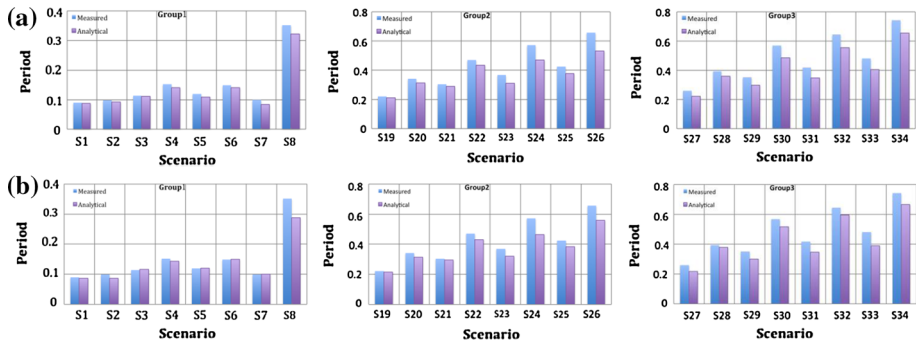
**Fig. 12** Comparison between the measured fundamental period $T_1$ and that obtained analytically $T_{1p}/T_{1pn}$ for: Group 1, Group 2 and Group 3, **a** $T_1/T_{1p}$, **b** $T_1/T_{1pn}$

SAP2000 simulations. The overall difference between the measured and calculated results is 0.097. For sub-figure group b, the differences between the results obtained experimentally and that by numerical modeling are even smaller. The average differences are 0.0426 (Group 1), 0.0983 (Group 2), and 0.1216 (Group 3). The overall difference is 0.0743. This verifies the excellent prediction accuracy of the proposed method by Luco (2013).

## 6 Research limitations in this work

In this research, the revised Dunkerley's formula introduced by Luco (2013) was testified both numerically and experimentally with excellent predicting accuracy, rendering it a valuable and useful input for future seismic code revisions. However there exist some limitations in this paper which are listed below:

(1) In the experiments the damping of the structure in each scenario was also obtained together with the fundamental period. Yet in response spectrum-based building codes, only the fundamental period is considered in evaluating the total seismic force of the structure, while the damping is often neglected in the procedure. Moreover, analyzing the smallest eigenvalue for a lightly damped system is the primary concern of the authors, which to our knowledge allows us to not incorporate damping in the calculations.

(2) The changes only in structural stiffness and mass were considered in the study, while other parameters (such as soil density, shear-wave velocity of the ground, slenderness ratio of the structure, torsional period of asymmetric/irregular structure, and the foundation embed types and configurations) were kept constant in the experiments due to budget limit.

The Dunkerley's formula introduced by Luco (2013) does not require the structural mass matrix to be diagonal. Further, when the coupling terms in the foundation impedance $k_{u\theta}$ cannot be neglected, and the mass and moment of inertia of the basement are not small compared to that of the superstructure, the revised Dunkerley's expression gives a more accurate prediction than the Jennings and Bielak (1973) or the Veletsos and Meek (1974) formulas, which is evidenced by the numerical parametric study in Luco (2013). This modified expression gives a better estimation of the range of possible SSI problems,

including flexible structures on light basements on stiff soils, flexible structures on flexible soils, as well as stiff structures on heavy and large basements on soft soils. In a word, the formula introduced by Luco could cover a wider spectrum of possible SSI problems with preferable predicting accuracy, so it can be applied to a broader range of researching areas in earthquake engineering.

Therefore, in order to further prove the accuracy of the formula presented by Luco (2013), it is recommended that future study may be focused by the interested readers on influence of the variation of these parameters, and the range of each parameter variation, on the fundamental period of the building with SSI.

# 7 Conclusions

A systematic experimental survey was performed on a 1/4-scale, steel-frame model building. Adding or removing inter-story diagonal struts and additional weights, respectively, could change the stiffness and mass of the structure. For the first time, the fixed-base fundamental periods of the structure were experimentally determined in different scenarios in order to avoid evaluation error in the conventional SSI analyses. Results obtained by using finite-element package (SAP2000®) were also given for comparison. A total of 34 different experimental scenarios were tested, and the fundamental periods and basic mode shapes were obtained.

An improved estimate using Dunkerley's method proposed by Luco (2013) was introduced in this investigation to predict the basic period of the structure with soil flexibility. It is found that the structure-to-soil relative stiffness $1/\sigma$ have the primary influence on SSI. With increasing $1/\sigma$, the period lengthening ratio $T_1/T$ increases significantly. The effect of structure-to-soil mass ratio on $T_1/T$ is not evident. The modal displacement amplitude of the base mat increases with increasing structure-to-soil stiffness $1/\sigma$.

The analytical basic periods of the structure with SSI was found in excellent agreement with that obtained both experimentally and numerically. The overall difference between the two is 0.097 and 0.0743, respectively. This shows that the improved estimate using Dunkerley's equation proposed by Luco can excellently predict the apparent period of the structure incorporating SSI. This validated formula has a wider application potential and preferable predicting accuracy than the existing expressions, and would be a useful reference for future seismic code revisions in assessing the basic period of the structure with SSI.

# 8 Video

The experimental video is available at: https://www.youtube.com/watch?v=kKXmYel-eEw&feature=youtu.be.

# References

ASCE (2005) Minimum design loads for buildings and other structures. American Society of Civil Engineers, Reston, VA

Avilés J, Pérez-Rocha LE (1999) Diagrams of effective periods and dampings of soil–structure systems. J Geotech Geoenviron Eng 125:711–715. doi:10.1061/(ASCE)1090-0241(1999)125:8(711)

Avilés J, Pérez-Rocha LE (2003) Soil–structure interaction in yielding systems. Earthq Eng Struct Dyn 32:1749–1771. doi:10.1002/eqe.300

Avilés J, Pérez-Rocha LE (2005) Influence of foundation flexibility on and factors. J Struct Eng 131:221–230. doi:10.1061/(ASCE)0733-9445(2005)131:2(221)

Avilés J, Suárez M (2002) Effective periods and dampings of building-foundation systems including seismic wave effects. Eng Struct 24:553–562. doi:10.1016/S0141-0296(01)00121-3

Bhattacharya K, Dutta SC (2004) Assessing lateral period of building frames incorporating soil-flexibility. J Sound Vib 269:795–821. doi:10.1016/S0022-460X(03)00136-6

Bielak J (1974) Dynamic behaviour of structures with embedded foundations. Earthq Eng Struct Dyn 3:259–274. doi:10.1002/eqe.4290030305

Gazetas G (1991) Formulas and charts for impedances of surface and embedded foundations. J Geotech Eng 117:1363–1381. doi:10.1061/(ASCE)0733-9410(1991)117:9(1363)

Hatzigeorgiou GD, Kanapitsas G (2013) Evaluation of fundamental period of low-rise and mid-rise reinforced concrete buildings. Earthq Eng Struct Dyn 42:1599–1616. doi:10.1002/eqe.2289

He Z, Shang S, Liu F, Xiong W (2008) Experimental study on fundamental frequency of soil–structure dynamic interaction system. J Railw Sci Eng 5:16–20

Jennings PC, Bielak J (1973) Dynamics of building–soil interaction. Bull Seismol Soc Am 63:9–48

Kausel E (2010) Early history of soil–structure interaction. Soil Dyn Earthq Eng 30:822–832. doi:10.1016/j.soildyn.2009.11.001

Khalil L, Sadek M, Shahrour I (2007) Influence of the soil–structure interaction on the fundamental period of buildings. Earthq Eng Struct Dyn 36:2445–2453. doi:10.1002/eqe.738

Ko Y-Y, Chen C-H (2009) Soil–structure interaction effects observed in the in situ forced vibration and pushover tests of school buildings in Taiwan and their modeling considering the foundation flexibility. Earthq Eng Struct Dyn 39:945–966. doi:10.1002/eqe.976

Kwon O-S, Kim ES (2010) Evaluation of building period formulas for seismic design. Earthq Eng Struct Dyn 39:1569–1583. doi:10.1002/eqe.998

Luco J (2013) Bounds for natural frequencies, Dunkerley's formula and application to soil–structure interaction. Soil Dyn Earthq Eng 47:32–37. doi:10.1016/j.soildyn.2012.08.007

Michel C, Zapico B, Lestuzzi P et al (2011) Quantification of fundamental frequency drop for unreinforced masonry buildings from dynamic tests. Earthq Eng Struct Dyn 40:1283–1296. doi:10.1002/eqe.1088

Shang S, Xiong W, Wang H et al (2009) SSI effects on the dynamic behavior of structures: experimental study on a 1/4 scaled steel-frame building prototype. China Civ Eng J 42:103–111

Stewart JP, Fenves GL, Seed RB (1999a) Seismic soil–structure interaction in buildings. I: analytical methods. J Geotech Geoenviron Eng 125:26–37. doi:10.1061/(ASCE)1090-0241(1999)125:1(26)

Stewart J, Seed R, Fenves G (1999b) Seismic soil–structure interaction in buildings. II: empirical findings. J Geotech Geoenviron Eng 125:38–48. doi:10.1061/(ASCE)1090-0241(1999)125:1(38)

Tileylioglu S, Stewart JP, Nigbor RL (2011) Dynamic stiffness and damping of a shallow foundation from forced vibration of a field test structure. J Geotech Geoenviron Eng 137:344–353. doi:10.1061/(ASCE)GT.1943-5606.0000430

Trifunac MD, Ivanović SS, Todorovska MI (2001a) Apparent periods of a building. II: time-frequency analysis. J Struct Eng 127:527–537. doi:10.1061/(ASCE)0733-9445(2001)127:5(527)

Trifunac MD, Ivanović SS, Todorovska MI (2001b) Apparent periods of a building. I: Fourier analysis. J Struct Eng 127:517–526. doi:10.1061/(ASCE)0733-9445(2001)127:5(517)

Trifunac MD, Todorovska MI, Manić MI, Bulajić BĐ (2010) Variability of the fixed-base and soil–structure system frequencies of a building—the case of Borik-2 building. Struct Control Health Monit 17:120–151. doi:10.1002/stc.277

Veletsos AS, Meek JW (1974) Dynamic behaviour of building-foundation systems. Earthq Eng Struct Dyn 3:121–138. doi:10.1002/eqe.4290030203

Veletsos AS, Nair VVD (1975) Seismic interaction of structures on hysteretic foundations. J Struct Div 101:109–129

Zaicenco A, Alkaz V (2007) Soil–structure interaction effects on an instrumented building. Bull Earthq Eng 5:533–547. doi:10.1007/s10518-007-9042-5